





RESEARCH ARTICLE OPEN ACCESS

Holocene Temperature Trend Inferred From Oxygen and Carbonate Clumped Isotope Profiles of a Stalagmite Collected From a Maritime Area of Central Honshu, Japan

Akira Murata¹  | Taiki Mori² | Hirokazu Kato³  | Hsun-Ming Hu^{4,5} | Chuan-Chou Shen^{4,5}  | Ryoko Senda⁶ | Kenji Kashiwagi⁷ | Akihiro Kano¹ 

¹Department of Earth and Planetary Science, Graduate School of Science, The University of Tokyo, Bunkyo-ku, Japan | ²Solution center, Chuo Kaihatsu Corporation, Kawaguchi, Japan | ³Faculty of Education and Human Science, Teikyo University of Science, Adachi-ku, Japan | ⁴High-Precision Mass Spectrometry and Environment Change Laboratory (HISPEC), Department of Geosciences, National Taiwan University, Taipei, Taiwan, ROC | ⁵Research Center for Future Earth, National Taiwan University, Taipei, Taiwan, ROC | ⁶Graduate School of Social and Cultural Studies, Kyushu University, Fukuoka, Japan | ⁷Faculty of Science, Toyama University, Toyama, Japan

Correspondence: Akira Murata (murakirasep@g.ecc.u-tokyo.ac.jp)

Received: 23 May 2024 | **Revised:** 18 November 2024 | **Accepted:** 6 December 2024

Funding: This study was supported by the Grant-in-Aids to Akihiro Kano (20H00191 and 23K17696) and Hirokazu Kato (24K07132) from the Ministry of Education, Culture, Sports, Science and Technology. U-Th dating was supported by research funds to Chuan-Chou Shen from the National Science and Technology Council, Taiwan (110-2123-M-002-009, 111-2116-M-002-022-MY3, and 111-2926-I-002-510-G), from Higher Education Sprout Project of the Ministry of Education, Taiwan (112L901001 [C.-C.S.]), and National Taiwan University (112L894202).

Keywords: carbonate clumped isotope | Holocene | oxygen isotopes | paleoclimate | stalagmite

ABSTRACT

The Holocene has been extensively researched concerning past climates, and various proxy records have provided information on temperature changes during this period. Many studies have found a period of elevated temperatures during the Middle Holocene, known as the Holocene Thermal Maximum (HTM). However, the exact timing of this warm period varies depending on the region. Here, we investigate a stalagmite collected from Kiriana Cave, which covers two intervals: 13.7–12.4 and 10.4–1.16 thousand years ago (ka before 1950 AD). In previous studies at this cave site, the meteoric water $\delta^{18}\text{O}$ is not sensitive to the precipitation amount and the seasonality of precipitation but follows the seawater $\delta^{18}\text{O}$. By using these assumptions of the meteoric water $\delta^{18}\text{O}$, the paleo-temperature was quantitatively reconstructed from the stalagmite $\delta^{18}\text{O}$ and the carbonate clumped isotopes. These paleoclimatic proxies indicated that the temperature at the cave site significantly changed during the Holocene. Based on the records of the stalagmite $\delta^{18}\text{O}$, the HTM occurred between 10.9 and 6.7 ka, reaching its peak temperature (15.0°C) around 7.0 ka. At this time, temperatures were approximately 3°C warmer than present. The timing of the warm interval aligns closely with marine temperature records but is notably earlier than terrestrial records from Europe and North America. Cooling began at 6.5 ka, and the decreased temperature stabilized in an interval between 6.0 and 4.5 ka. The temperature decreased further to the lowest value (~10.0°C) at 3.0 ka. After this cooling maximum, the climate gradually became warm until the stalagmite stopped growing at 1.16 ka. Our Holocene temperature reconstruction is consistent with the temperature and palaeoceanographic records obtained from reef corals and marine sediments in and around the Japanese Islands in terms of the amplitude of change, warm middle Holocene, and cool late Holocene.

This is an open access article under the terms of the [Creative Commons Attribution-NonCommercial-NoDerivs](https://creativecommons.org/licenses/by-nc-nd/4.0/) License, which permits use and distribution in any medium, provided the original work is properly cited, the use is non-commercial and no modifications or adaptations are made.

© 2024 The Author(s). *Island Arc* published by John Wiley & Sons Australia, Ltd.

1 | Introduction

Stalagmite-stable oxygen isotope ratio ($\delta^{18}\text{O}$) records have significantly contributed to our understanding of late Pleistocene and Holocene paleoclimatology, becoming a global standard for terrestrial climate change (Cheng et al. 2016; Walker et al. 2018). The $\delta^{18}\text{O}$ profiles of Chinese stalagmites have revealed that millennial-scale oscillations correlated with the changes in ice-sheet $\delta^{18}\text{O}$ records (Wang et al. 2001), along with a long-term trend broadly corresponding to summer solar insolation in Northern Hemisphere (Wang et al. 2008). The linkage between climate and stalagmite $\delta^{18}\text{O}$ has been largely attributed to the $\delta^{18}\text{O}$ of local meteoric water. Temperature plays a subsidiary role in controlling stalagmite $\delta^{18}\text{O}$ and does not fully explain the large amplitude of the change observed in the Chinese stalagmites. For example, the lowered $\delta^{18}\text{O}$ signals in the mid-Holocene likely resulted from a decreased meteoric water $\delta^{18}\text{O}$, rather than an increased temperature (Wang et al. 2001, 2008).

The climatic factor driving the decreased meteoric water $\delta^{18}\text{O}$ in China remains controversial. One popular interpretation is the amount effect, where heavy rainfall generally leads to lower $\delta^{18}\text{O}$ signals. According to this viewpoint, the intensified East Asian summer monsoon (EASM) during the mid-Holocene increased precipitation amounts and decreased meteoric water $\delta^{18}\text{O}$ (e.g., Wang et al. 2001, 2008; Cheng et al. 2016). An alternative interpretation considers the relative contribution of ^{18}O -enriched moisture from the EASM and ^{18}O -depleted moisture from the Indian monsoon (e.g., Pausata et al. 2011; Liu et al. 2014; Wang et al. 2014; Yang et al. 2014). Additionally, previous studies in Europe, the United States, and Japan have proposed other potential controls to the meteoric water $\delta^{18}\text{O}$, such as a change in moisture recycling over land (Baker et al. 2019), soil water evaporation in dry climate zones (Fairchild et al. 2006), and the water $\delta^{18}\text{O}$ of moisture source (Bar-Matthews et al. 2003; Amekawa et al. 2021). The global meteoric water database suggested that the distance from the coast and the air temperature are also important factors for the meteoric water $\delta^{18}\text{O}$ (Dansgaard 1964; Rozanski, Araguás-Araguás, and Gonfiantini 1993).

Views on stalagmite $\delta^{18}\text{O}$ were re-examined by the records from maritime Japan, located in the eastern part of the Asian monsoon region beyond the influence of the Indian monsoon (Shen et al. 2010; Hori et al. 2013; Mori et al. 2018). Japanese stalagmites display temporal patterns of the $\delta^{18}\text{O}$ signals similar to those of the Chinese records but with unique features. The most distinct difference from the Chinese records lies in the amplitude of the changes (Kano, Kato, and Murata 2023). The Japanese stalagmite $\delta^{18}\text{O}$ profiles show a clearly smaller amplitude compared with the Chinese stalagmites. For example, the $\delta^{18}\text{O}$ shift from the last glacial maximum (LGM) to the mid-Holocene is $\sim 5\text{‰}$ in China, but only $\sim 2\text{‰}$ in Maboroshi Cave in Hiroshima (Hori et al. 2013) and less than 3‰ in Kiriana Cave in Mie Prefecture (Mori et al. 2018). Another feature is the similarity with the $\delta^{18}\text{O}$ trend of the seawater, as demonstrated by the long-term trend of the Kiriana stalagmite, KA03, for the last 84 kyr (Mori et al. 2018). This is reasonable because seawater is the dominant moisture source for maritime Japan. The shift of the seawater $\delta^{18}\text{O}$ corresponds

to $\sim 40\%$ of the shift of the stalagmite $\delta^{18}\text{O}$ between LGM and mid-Holocene of KA03. The remaining 1.8‰ in the difference can be accounted for by a 9°C increase in temperature (Mori et al. 2018), consistent with paleoclimate studies using stalagmites, lake deposits, and marine deposits around the Japanese Islands (Nakagawa et al. 2002; Kawahata, Ohshima, and Kuroyanagi 2011; Kigoshi et al. 2014; Uemura et al. 2016; Kato et al. 2021, 2023). Thus, the stalagmite $\delta^{18}\text{O}$ record from Kiriana Cave was likely a superimposed signal of variations in the air temperature and the seawater $\delta^{18}\text{O}$, rather than the climate-induced hydrodynamic control on meteoric water $\delta^{18}\text{O}$ (Kano, Kato, and Murata 2023). Mori et al. (2018) concluded that these features were due to the geographic position of Kiriana near the moisture source, the Kuroshio warm current. Novel approaches, such as clumped isotopes, can help to estimate the hydrodynamic and temperature effects of $\delta^{18}\text{O}$.

Stalagmites from Kiriana Cave are potential temperature recorders. However, only a 9-cm long KA03 is a slow-grown stalagmite (Mori et al. 2018) and has difficulty obtaining high-resolution records from its 1.7-cm-long Holocene section. In this study, we report stalagmite KA01, 34.5-cm-long, collected from Kiriana Cave, which provides higher-resolution $\delta^{18}\text{O}$ records during the Holocene. Based on the $\delta^{18}\text{O}$ and carbonate clumped isotope records of KA01, and the assumptions of Mori et al. (2018) and Kano, Kato, and Murata (2023), we discuss Holocene temperatures in the maritime Japanese Islands.

2 | Materials and Methods

2.1 | Climate Settings and Meteoric Water $\delta^{18}\text{O}$

Kiriana Cave ($34^\circ 37' \text{N}$, $136^\circ 46' \text{E}$; altitude 620 m) in Mie Prefecture is located 20 km from the coastline of the mountainous Kii Peninsular in central Honshu (Figure 1A). The nearest meteorological observatory at Kayumi (altitude: 120 m) recorded an annual average precipitation of 2131 mm/year during 1991–2020 A.D. The regional climate is characterized by a clear seasonal contrast in rainfall at this site, with 75% of the annual amount falling during the warm 6 months (May–October; Figure 1B) when the wet westerly and southerly winds blow from the Pacific Ocean. The 30-year mean annual temperature is 14.8°C , with the monthly temperature ranging from 4.2°C in January to 26.1°C in August (Figure 1B). Considering the altitude difference between Kayumi and Kiriana (500 m) and a temperature gradient of $0.6^\circ\text{C}/100 \text{ m}$, the average temperature at Kiriana Cave can be estimated at 11.8°C . Figure 1C shows a long-term change in the annual temperature at Owase weather observatory since 1939 A.D., indicating an approximately 2°C warming. The average temperature of the last 30 years (16.5°C) is 1.1°C higher than the average temperature before (15.4°C , Figure 1C). Therefore, the air temperature at Kiriana Cave is estimated to be around 10.7°C in the pre-industrial ages.

Samples of 144 rain events collected at Ohdai (altitude: 120 m, 7 km northwest of the Kiriana Cave; Table S1) display a wide range of $\delta^{18}\text{O}$ values from -0.1‰ (December 15, 2015) to -29.0‰ (April 27, 2016; Mori et al. 2018). The $\delta^{18}\text{O}$ value of rainwater shows no correlation with the total amount of

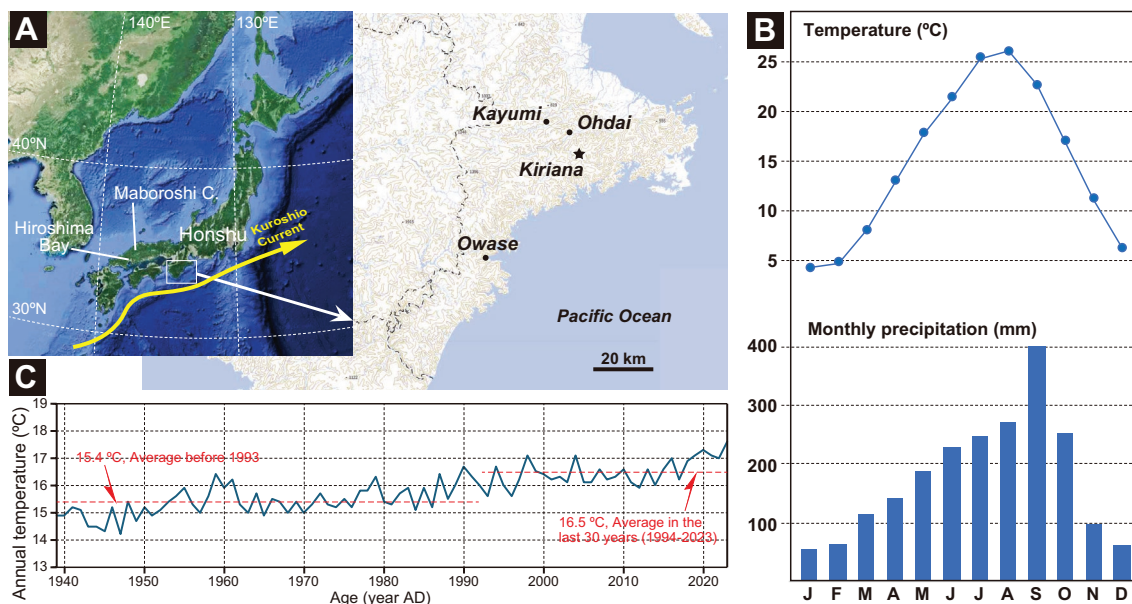


FIGURE 1 | Geographic and climatological settings of the study area. (A) Map showing study sites. Dotted lines indicate the prefectural borders. (B) Average monthly temperature and precipitation of the recent 30 years (1991–2020) at Kayumi, the nearest weather observatory from the Kiriana Cave. (C) Annual temperature of the last 85 years (1939–2023) at Owase, the weather observatory with the longest record near Kiriana Cave.

rainfall ($R = -0.02$, $p = 0.79$; Figure 2A) or with air temperature ($R = -0.03$, $p = 0.66$; Table S1), based on weather data from the Kayumi weather observatory in the Japan Meteorological Agency database. Monthly averages of $\delta^{18}\text{O}$ values weighted by the precipitation amount are highest in August (-6.0‰) and lowest in January (-11.7‰) (Figure 2B). There is no distinct seasonal pattern; the weighted average of some months is influenced by heavy rain events with distinct $\delta^{18}\text{O}$ values, such as on August 25, 2015 (340 mm, -4.3‰) and October 22, 2017 (468 mm, -10.0‰). The total weighted average $\delta^{18}\text{O}$ value over the collection period is -8.1‰ .

Kano, Kato, and Murata (2023) conducted a model calculation to examine the amount effect and the seasonality of meteoric water $\delta^{18}\text{O}$ at four Japanese localities including Ohdai near Kiriana Cave (Figure 1A). Their method selected an appropriate number of rainfall events from the rainwater samples until the total amount reached the actual range of the annual precipitation. Then, they calculated the total amount of precipitation, the weighted average of $\delta^{18}\text{O}$, and the winter rainfall ratio (percentage of precipitation from November to April in the annual precipitation) of a virtual year. Results of 600 virtual years for Ohdai show that the weighted average of $\delta^{18}\text{O}$ is not correlated well with the annual amount of precipitation ($R = 0.21$, $p < 0.001$; Figure 2C) and with the winter rainfall ratio ($R = -0.22$, $p < 0.001$; Figure 2D, see Supporting Information of Kano, Kato, and Murata (2023)).

2.2 | Kiriana Cave and Stalagmite KA01

The studied cave, Kiriana, is approximately 2 km long and 200 m in depth and developed in the Triassic limestone bedrock of the southern Chichibu Terrane (Kashiwagi, Yoshida, and Inagaki 2007; Suzuki et al. 2015). Stalagmites are found at several locations along horizontal passages situated beneath a

vertical hole that descends 50 m deep. Dripwater samples were collected at six sites in Kiriana Cave, in four seasons (March, June, September, and December) of the year 2015 (Mori et al. 2018). The average $\delta^{18}\text{O}$ values of dripwater range relatively uniformly from -6.72‰ (June) to -7.07‰ (December) (red stars in Figure 2B). The average dripwater value of -6.90‰ is 1.18‰ higher than the average rainwater value at Ohdai. This discrepancy can be attributed to the positions along the dominant moisture transportation route in the Kii Peninsula. Moisture transported by southerly winds first precipitates as relatively ^{18}O -enriched rain at Kiriana, located on the southeastern slope of the peninsula, before bringing ^{18}O -depleted rain to inland locations including Ohdai. A study on the spatial distribution of the surface water $\delta^{18}\text{O}$ in the Kii Peninsula clearly demonstrates this geographic effect, showing ^{18}O enrichment on the southeast coast and ^{18}O depletion in inland areas (Ishizuka et al. 2004). The dripwater in the Kiriana contains relatively low calcium ions, generally 30–35 mg/L (Mori et al. 2018), which is not enough to precipitate calcium carbonate (e.g., Kano et al. 2019).

The studied stalagmite sample KA01 was collected in a chamber with humidity from 95% to 100%, 220-m distance from a cave entrance. This stalagmite measures 345 mm in length and consists of relatively pure calcite. Its section shows a heterogeneous internal texture, opaque in the upper 70 mm and transparent in the lower 275 mm (Figure 3A). The transparent part also exhibits distinct laminae at several levels, such as 94.5, 116.5, 194.0, and 292.5 mm from the top.

2.3 | Dating

The ages of KA01 were determined using ^{230}Th dating techniques (Shen et al. 2008, 2012) at the National Taiwan University. Seventeen layers of the polished surface of

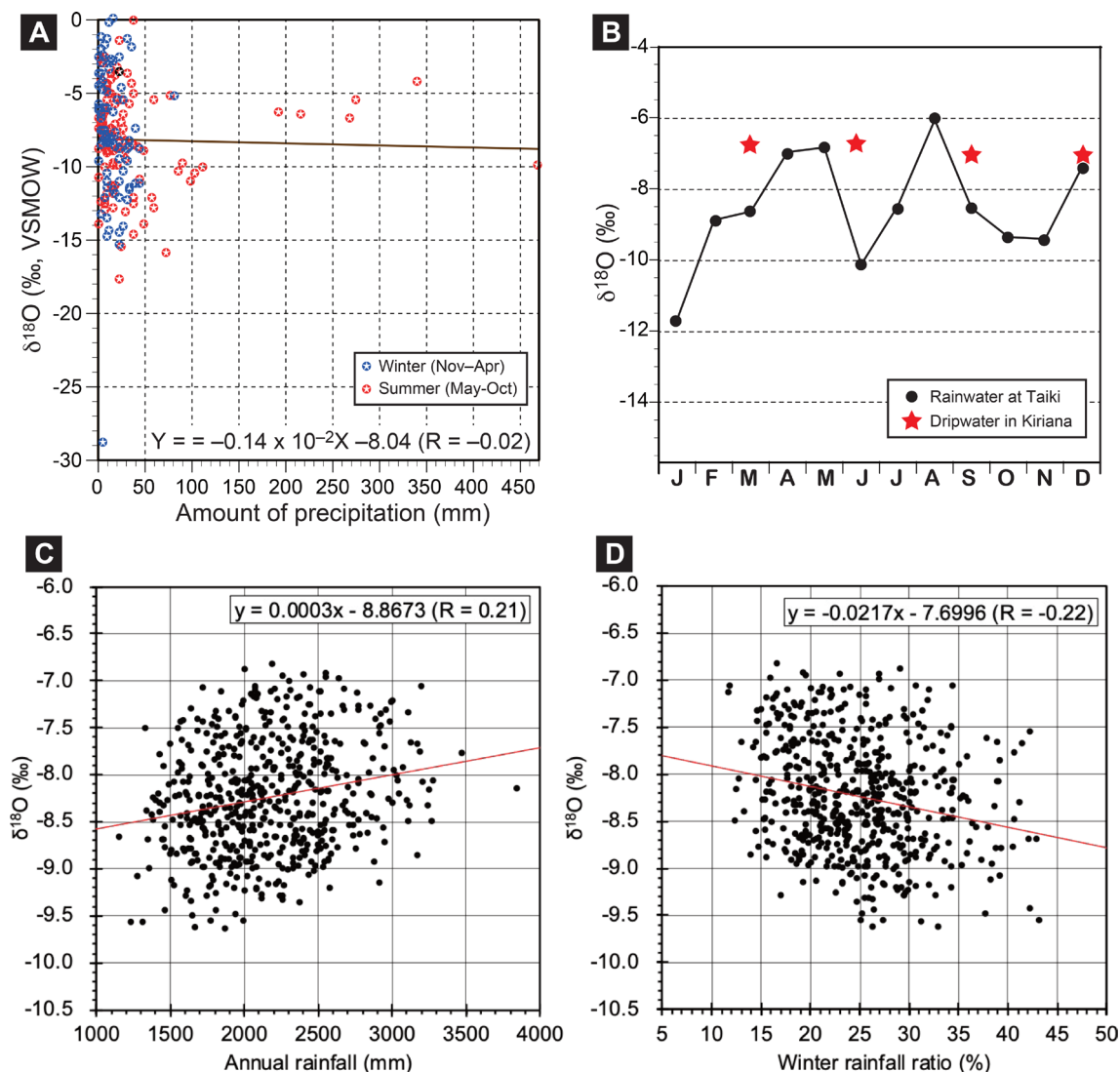


FIGURE 2 | Oxygen isotopic composition of the rainwater samples collected from Ohdai. (A) $\delta^{18}\text{O}$ (‰) and the amount of rainfall (mm) of 144 rainwater samples (data are available in Table S1). (B) Monthly weighted average of the rainwater $\delta^{18}\text{O}$. (C) Result of the model calculation showing the relationship between $\delta^{18}\text{O}$ and the annual amount of precipitation. (D) Result of the model calculation showing the relationship between $\delta^{18}\text{O}$ and the winter (November–April) rainfall ratio.

stalagmite KA01 were sampled, with an amount of 100–200 mg for U–Th chemistry (Shen et al. 2002). These samples underwent dissolution with 5% nitric acid and were spiked with an artificial radiometric tracer (^{229}Th – ^{233}U – ^{236}U). A Fe^{3+} solution was then added to the solution to remove Ca^{2+} through iron coprecipitation. Subsequently, U and Th fractions were purified using anion exchange chromatography. The isotopic composition of U and Th was measured using a multicollector inductively coupled plasma mass spectrometer (MC-ICP-MS), Thermo Electron NEPTUNE at National Taiwan University. Details of the chemical treatment and instrumental analysis are shown in Shen et al. (2012). Decay constants used for age calculation are given in Cheng et al. (2013) and Jaffey et al. (1971). The age was corrected by the estimation of contaminated detrital ^{230}Th . An age–depth model was constructed using the StalAge software, which adopts a statistical algorithm based on Bayesian and Monte Carlo simulations (Scholz and Hoffmann 2011).

2.4 | Stable Isotope Analysis

Stable isotope analysis was conducted using a mass spectrometer (Thermo Finnigan DeltaPlus) connected to an online gas separation system (GasBench II) at the University of Tokyo. A total of 1712 subsamples were collected along the growth axis with a dental microdrill (Shofu Tas-35LX) at intervals of 0.2 mm (Figure 3A). In addition, a Hendy test that examines the stability of $\delta^{18}\text{O}$ value along the same growth layer (Hendy 1971) was also performed for four horizons. Seven subsamples were collected along each horizon at 1-mm intervals on both sides from the growth axis.

Each subsample of ~0.3 mg was enclosed in a 12-mL gastight vial, with the air replaced by helium gas. The subsamples were reacted with phosphoric acid in the vial for over 5 h at 60°C. The generated CO_2 was then introduced to the gas separation system and the mass spectrometer. $\delta^{18}\text{O}$ and stable carbon isotope ratio

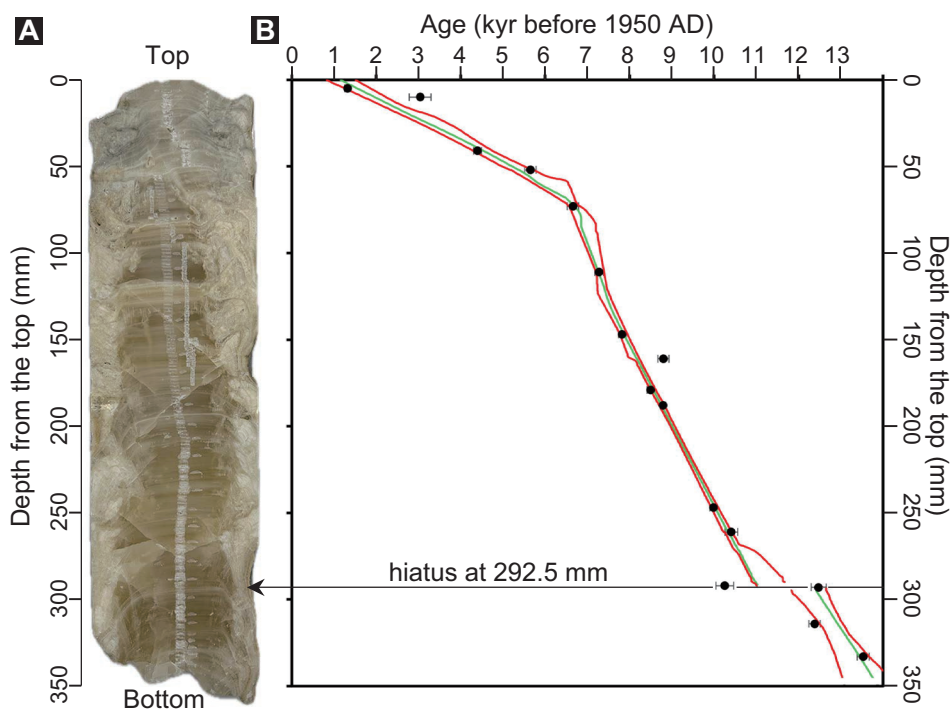


FIGURE 3 | Basic information of the stalagmite KA01 collected from the Kiriana Cave. (A) Polished surface of a half-cut specimen. (B) Age model of KA01 based on 17 ^{230}Th ages (Table 1). Calculation by using StalAge (Scholz and Hoffmann 2011) provides the mean age (green line) and maximum and minimum ages (red lines). A hiatus was identified at a 292.5-mm horizon corresponding to a distinct lamina in Figure 3A.

($\delta^{13}\text{C}$) values were normalized using the value of an in-house standard and expressed with the Vienna Pee Dee Belemnite standard (VPDB). A typical 2 standard error (SE) is 0.2‰ for both $\delta^{18}\text{O}$ and $\delta^{13}\text{C}$. The reproducibility of the measurements of in-house standard ($N=344$) was $\pm 0.09\text{‰}$ (2SD). Further details of $\delta^{18}\text{O}$ and $\delta^{13}\text{C}$ measurements were described by Hori et al. (2009).

2.5 | Carbonate Clumped Isotope

Carbonate clumped isotope of 19 horizons of KA01 was measured using a dual inlet mass spectrometer (Finnigan MAT-253) at Kyushu University. Powdered samples of 5 mg were reacted with phosphoric acid at 90°C in a vacuumed glass tube, and the generated CO_2 and H_2O were immediately trapped by a stainless tube cooled with liquid nitrogen. The H_2O was trapped with ethanol slush, while the gaseous CO_2 was purified by passing it through a gas chromatography with helium gas. A 30-m-long capillary column (Supel-Q PLOT), cooled at -10°C , was used in order to remove organic contaminants.

The purified CO_2 was analyzed by applying the pressure baseline (PBL) correction by He, Olack, and Colman (2012), incorporating an off-peak measurement of the background intensities of masses 45–49. Each analysis comprises 5–8 acquisitions, with four off-peak, eight on-peak, and four off-peak cycles (sample-reference comparisons) per acquisition, taking approximately 3.5 h. A typical 1 SE of the abundance anomaly of $^{47}\text{CO}_2$ (Δ_{47}) is 0.005‰–0.015‰. The Δ_{47} value was converted to temperature using the following equation for synthetic calcite proposed by Kato et al. (2019):

$$\Delta_{47} = (0.0354 \pm 0.0013) \times 10^6 / T^2 + (0.290 \pm 0.015) \quad (1)$$

3 | Results

3.1 | U–Th Dating and Age-Depth Model

U–Th ages from 17 horizons of KA01 range from 1.33 to 13.53 kyr (before 1950 AD; Table 1). Two ages at depths of 10 and 161 mm are clearly out of stratigraphic order and were not applied in the construction of the age-depth modeling StalAge, where linearity is important. The remaining 15 dates were applied to the age model created by StalAge (Figure 3B). According to this age model, the ages of the top and the bottom are estimated to be 1.16 and 13.69 ka, respectively. A significant age gap was identified between the two samples at the 292- and 293-mm horizons, which were dated to approximately 10.25 and 12.47 ka, respectively. These two samples are separated by a distinct lamina at the 292.5-mm horizon (Figure 3A), which is identified as a hiatus. This estimated hiatus is 1300 years long, occurring between 12.35 and 11.05 ka.

The age model of KA01 is approximated with three linear relationships with different slopes, indicating various stalagmite growth rates (Figure 3B). The uppermost 72.5 mm has the lowest growth rate (~ 13 mm/kyr). The interval of 72.5–292.5 mm exhibits a higher growth rate (~ 50 mm/kyr). The bottom section below the hiatus shows a growth rate of ~ 33 mm/kyr.

3.2 | Stable Oxygen Isotopes

The $\delta^{18}\text{O}$ values of the KA01 ranged from -5.46‰ to -7.52‰ (Table S2), with a mean value of -6.43‰ . Figure 4A displays the raw data (light green) and the 50-year average of every 25-year time slice (dark green; Table S3). The $\delta^{18}\text{O}$ values differ depending on

TABLE 1 | U-Th isotopic compositions and estimated ages of 17 horizons of the stalagmite KA01 collected from Kiriana Cave, central Japan.

Horizon mm	Weight g	^{238}U		^{232}Th		$\delta^{234}\text{U}$		$[\text{}^{230}\text{Th}/\text{}^{238}\text{U}]$		$[\text{}^{230}\text{Th}/\text{}^{232}\text{Th}]$		Age (kyr ago)		Age (ka)		$\delta^{234}\text{U}_{\text{initial}}$	
		$10^{-9}\text{g/g}^{\text{a}}$		10^{-12}g/g		Measured ^a		Activity ^c		Atomic ($\times 10^{-6}$)		Uncorrected		Corrected ^{c,d}		Corrected ^b	
5	0.1463	30.852 ± 0.032		180.2 ± 3.2		286.9 ± 1.8		0.01697 ± 0.00047		47.9 ± 1.6		1.446 ± 0.040		1.326 ± 0.072		288.0 ± 1.8	
10	0.0621	30.674 ± 0.059		684.6 ± 7.6		284.6 ± 3.5		0.04062 ± 0.00136		30.0 ± 1.1		3.500 ± 0.119		3.040 ± 0.259		287.1 ± 3.6	
41	0.1019	45.272 ± 0.067		281.5 ± 4.6		278.8 ± 2.9		0.05202 ± 0.00076		137.9 ± 3.0		4.522 ± 0.068		4.394 ± 0.094		282.3 ± 2.9	
51.5	0.1846	40.674 ± 0.105		415.8 ± 2.7		304.8 ± 3.7		0.06839 ± 0.00095		110.3 ± 1.7		5.859 ± 0.085		5.653 ± 0.134		309.7 ± 3.8	
72.5	0.1011	45.748 ± 0.122		410.0 ± 4.6		265.9 ± 4.9		0.07717 ± 0.00099		142.0 ± 2.4		6.845 ± 0.094		6.658 ± 0.132		270.9 ± 5.0	
111	0.1065	61.430 ± 0.095		95.5 ± 4.4		296.8 ± 3.5		0.08371 ± 0.00108		887.8 ± 42.1		7.306 ± 0.104		7.276 ± 0.105		302.9 ± 3.5	
147	0.1097	40.722 ± 0.077		110.5 ± 4.2		341.2 ± 3.6		0.09370 ± 0.00095		569.5 ± 22.6		7.875 ± 0.085		7.822 ± 0.089		348.8 ± 3.7	
161	0.1145	47.160 ± 0.067		359.3 ± 4.1		322.9 ± 2.4		0.10457 ± 0.00119		226.3 ± 3.6		8.951 ± 0.107		8.799 ± 0.131		331.0 ± 2.5	
178.5	0.1139	43.998 ± 0.060		114.2 ± 4.1		322.7 ± 2.3		0.10007 ± 0.00093		635.5 ± 23.4		8.552 ± 0.084		8.500 ± 0.088		330.6 ± 2.3	
188	0.0978	45.792 ± 0.044		53.9 ± 4.7		329.9 ± 1.9		0.10356 ± 0.00074		1450.3 ± 128.1		8.812 ± 0.067		8.789 ± 0.068		338.2 ± 1.9	
247	0.1163	55.588 ± 0.108		159.7 ± 4.0		366.1 ± 3.2		0.12061 ± 0.00088		692.2 ± 18.0		10.040 ± 0.080		9.985 ± 0.085		376.5 ± 3.3	
261	0.1020	46.056 ± 0.066		525.6 ± 4.7		382.3 ± 2.6		0.12884 ± 0.00122		186.2 ± 2.4		10.623 ± 0.107		10.406 ± 0.152		393.7 ± 2.7	
292	0.1086	31.530 ± 0.039		122.6 ± 4.3		423.1 ± 2.1		0.12911 ± 0.00250		547.7 ± 21.9		10.325 ± 0.210		10.253 ± 0.212		435.5 ± 2.1	
293	0.0542	27.094 ± 0.034		353.7 ± 8.6		442.7 ± 3.5		0.15958 ± 0.00156		201.5 ± 5.3		12.709 ± 0.136		12.472 ± 0.180		458.6 ± 3.7	
304	0.1084	28.435 ± 0.043		116.0 ± 4.3		507.8 ± 3.1		0.15885 ± 0.00177		642.0 ± 24.8		12.066 ± 0.144		11.996 ± 0.148		525.3 ± 3.2	
314	0.1163	40.559 ± 0.077		301.2 ± 4.0		471.8 ± 5.0		0.16042 ± 0.00135		356.2 ± 5.6		12.510 ± 0.120		12.378 ± 0.137		488.6 ± 5.2	
333	0.1230	38.924 ± 0.041		469.2 ± 3.8		508.8 ± 2.1		0.17974 ± 0.00120		245.8 ± 2.6		13.737 ± 0.099		13.528 ± 0.144		528.6 ± 2.2	

Note: Analytical errors are 2σ of the mean. Decay constants used for age calculation are listed in Cheng et al. (2013). Those are the values for a material at secular equilibrium, with a crustal $^{232}\text{Th}/^{238}\text{U}$ value of 3.8. The errors are arbitrarily assumed to be 50%.

^a $[\text{}^{235}\text{U}]/[\text{}^{238}\text{U}] \times 137.818 (\pm 0.65\%)$ (Hess et al. 2012); $\delta^{234}\text{U} = ([\text{}^{234}\text{U}/\text{}^{238}\text{U}]_{\text{activity}} - 1) \times 1000$.

^b $\delta^{234}\text{U}_{\text{initial}}$ corrected was calculated based on ^{230}Th age (T), that is, $\delta^{234}\text{U}_{\text{initial}} = \delta^{234}\text{U}_{\text{measured}} \times e^{(\lambda^{234}\text{U} - \lambda^{230}\text{Th})T}$, where T is the age.

^c $[\text{}^{230}\text{Th}/\text{}^{238}\text{U}]_{\text{activity}} = 1 - e^{-\lambda^{230}\text{Th}T} + (\delta^{234}\text{U}_{\text{measured}}/1000)/(\lambda^{230}\text{Th} - \lambda^{234}\text{U})[1 - e^{-(\lambda^{230}\text{Th} - \lambda^{234}\text{U})T}]$, where T is the age.

^dAge corrections, relative to AD 1950, for samples were calculated using an estimated atomic $^{230}\text{Th}/^{232}\text{Th}$ ratio of $4 (\pm 2) \times 10^{-6}$.

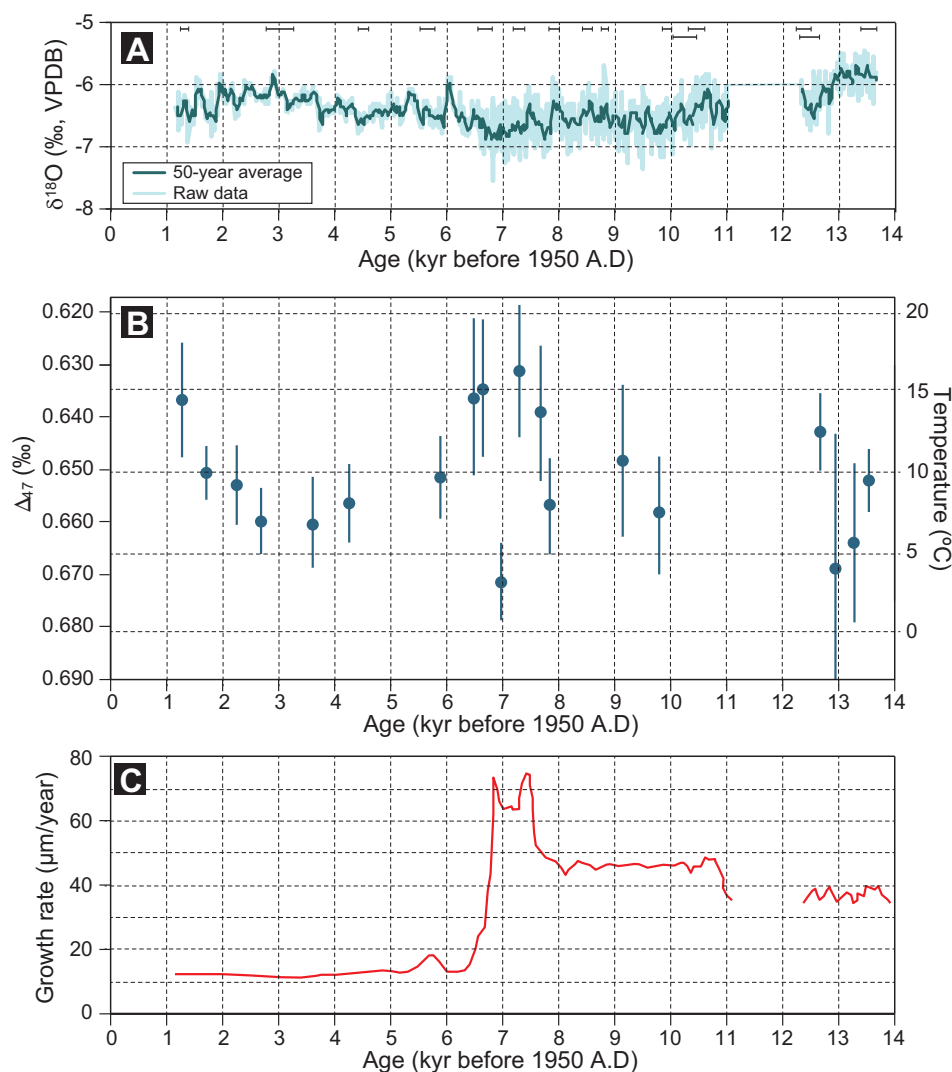


FIGURE 4 | Results of isotopic analyses of KA01. (A) Raw data values (light green) and average values in a 25-year time slice of $\delta^{18}\text{O}$ (dark green). (B) Carbonate clumped isotopes and estimated temperatures of 19 horizons of KA01 (data are shown in Table 2). (C) Growth rate of KA01 calculated from the age model of Figure 3B.

positions in the stalagmite. High values ($> -6\text{‰}$) are recorded in the lowermost part (13.7–12.35 ka) and also in the uppermost part (3.0–1.16 ka), while the middle part of the stalagmite (11.05–6.3 ka) generally exhibits low $\delta^{18}\text{O}$ values around -6.5‰ . The $\delta^{18}\text{O}$ profile of the upper stalagmite (6.3–1.16 ka) shows centennial-scale oscillations with an amplitude of $< 0.5\text{‰}$ (Figure 4A).

The results of Hendy tests conducted at 20-, 90-, 170-, and 330-mm horizons are shown in Figure S1. For $\delta^{18}\text{O}$, the values at seven positions are mostly within the margin of analytical error (the average $\pm 0.20\text{‰}$). The $\delta^{13}\text{C}$ values indicate larger perturbation, $\pm 0.25\text{‰}$ for 20- and 90-mm horizons and $\pm 0.50\text{‰}$ for 170- and 330-mm horizons.

3.3 | Carbonate Clumped Isotopes

Table 2 and Figure 4B show the results of the carbonate clumped isotopes from 19 horizons. The Δ_{47} values range from 0.6309‰ to 0.6686‰, which corresponds to the temperature range of 16.2°C–4.1°C. The analytical error (1 SD) is from 0.0052‰ to

0.0217‰, indicating the uncertainty from $\pm 1.7^\circ\text{C}$ to $\pm 6.8^\circ\text{C}$ (Table 2).

Relatively high temperatures (13.6°C–16.2°C) are obtained in a time interval between 7.8 and 6.5 kyr (before 1950 AD). However, the temperature at 7.1 ka is the lowest at 3.4°C. Temperatures lower than 10°C occur in intervals of 13.6–13.0 ka and 6.0–1.8 ka. Additionally, low temperatures are recorded at 9.9 and 7.9 ka (Table 2).

4 | Discussion

4.1 | Interpretation of Oxygen Isotopes

The stalagmite oxygen isotopes are basically controlled by two factors: (1) $\delta^{18}\text{O}$ of the dripwater, which principally originated from the meteoric water, and (2) the temperature during calcite precipitation (e.g., Kano, Kato, and Murata 2023). As observed in caves elsewhere in the world (e.g., McDermott 2004), the first factor is generally more important than the second

TABLE 2 | Carbonate clumped isotopes, estimated temperatures, and growth rates of 19 horizons of KA01.

Horizon (mm)	Age (yb 1950)	$\delta^{13}\text{C}$ (‰)	$\delta^{18}\text{O}$ (‰)	Δ_{47} (‰)	Temperature (°C)	Growth rate ($\mu\text{m}/\text{year}$)	Δ_{48} (‰)
2.6	1356	−7.01	−6.02	0.6365 ± 0.0111	14.3 ± 3.8	12.3	-0.8945 ± 0.2896
8.2	1816	−8.44	−6.55	0.6503 ± 0.0052	9.8 ± 1.7	12.1	-0.9927 ± 0.1925
15.0	2373	−8.30	−5.92	0.6526 ± 0.0076	9.1 ± 2.4	12.2	-0.8198 ± 0.3936
20.0	2786	−8.32	−6.32	0.6597 ± 0.0064	6.8 ± 2.0	11.9	-1.1846 ± 0.1944
30.5	3689	−9.57	−6.45	0.6602 ± 0.0088	6.7 ± 2.8	12.0	-0.6199 ± 0.4307
39.0	4380	−9.23	−6.23	0.6562 ± 0.0076	7.9 ± 2.4	12.7	-0.8177 ± 0.2327
62.0	6005	−7.28	−6.09	0.6513 ± 0.0080	9.5 ± 2.6	13.2	-1.1943 ± 0.3981
70.0	6567	−8.33	−6.35	0.6361 ± 0.0152	14.4 ± 5.2	23.5	-1.3132 ± 0.5227
75.0	6761	−8.49	−6.45	0.6344 ± 0.0133	15.0 ± 4.6	25.9	-1.1957 ± 0.4239
98.4	7065	−9.17	−6.25	0.6711 ± 0.0075	3.4 ± 2.3	63.8	-0.9114 ± 0.3828
121.0	7409	−8.46	−6.61	0.6309 ± 0.0128	16.2 ± 4.5	81.5	-1.3969 ± 0.4705
142.2	7765	−9.56	−6.35	0.6387 ± 0.0131	13.6 ± 4.5	48.5	-0.4582 ± 0.3261
151.0	7948	−8.52	−6.36	0.6564 ± 0.0093	7.9 ± 3.0	47.0	-0.9567 ± 0.3364
210.0	9227	−8.10	−6.43	0.6481 ± 0.0147	10.5 ± 4.9	46.5	-0.6199 ± 0.4307
240.0	9873	−9.53	−6.89	0.6578 ± 0.0114	7.4 ± 3.6	46.7	-1.2228 ± 0.2970
308.8	12786	−10.42	−6.61	0.6425 ± 0.0075	12.3 ± 2.5	39.4	-1.0011 ± 0.2933
318.6	13052	−8.80	−6.59	0.6686 ± 0.0217	4.1 ± 6.8	38.5	-0.0975 ± 1.6101
329.0	13339	−9.11	−6.51	0.6636 ± 0.0154	5.6 ± 4.8	39.4	-1.3318 ± 0.2983
341.1	13654	−8.91	−6.63	0.6517 ± 0.0061	9.3 ± 2.0	40.1	-0.9415 ± 0.3127

factor. However, this cannot simply be applied to Japanese stalagmites.

As described above, Kano, Kato, and Murata (2023) examined the amount effect and the seasonality of the meteoric water $\delta^{18}\text{O}$ by using a dataset of the meteoric water $\delta^{18}\text{O}$, which was collected from several sites, including Ohdai, which is close to Kiriana Cave. According to this study, the meteoric water $\delta^{18}\text{O}$ at Ohdai has no significant correlation with the annual amount of rainfall (Figure 2C) and with the winter rainfall ratio (Figure 2D). As this locality is only 20 km from the coastline (Figure 1A), moisture mostly comes from the Pacific. Wet air masses from west and south bring ^{18}O -enriched rainfall along a short trajectory on the southern slope of the Kii Peninsula. Therefore, the degree of rainout of ^{18}O -enriched H_2O along the moisture trajectory is likely insignificantly related to the intensity of rainfall. $\delta^{18}\text{O}$ of heavy rain can be as low as -10‰ (October 22, 2017; 468 mm) but as high as -4.3‰ (August 25, 2015; 340 mm). In addition, 75% of the annual rainfall occurs from May to October (Figure 1B) when the westerly and southerly winds bring moisture from the Pacific Ocean. Because of the minor contribution of rainfall during cold months, changes in rainfall seasonality do not largely influence the meteoric water $\delta^{18}\text{O}$.

A small range of variation is a characteristic of the stalagmite $\delta^{18}\text{O}$ of the Kiriana Cave. This was previously suggested for the stalagmite KA03, which covers a longer age range (4–83 ka)

than KA01 (Mori et al. 2018). The $\delta^{18}\text{O}$ profile of KA03 has only $\sim 2\text{‰}$ variation in amplitude and shows a long-term trend similar to seawater $\delta^{18}\text{O}$. Because seawater is the dominant moisture source at this cave on the centennial to millennial timescale, it is reasonable to infer that the variation of the meteoric water and stalagmite $\delta^{18}\text{O}$ is inherited from the seawater $\delta^{18}\text{O}$. Subtraction of the seawater $\delta^{18}\text{O}$ variation further reduces the amplitude of the stalagmite $\delta^{18}\text{O}$ variation, which can be interpreted as temperature change (Mori et al. 2018).

4.2 | Reconstruction of Temperature Change

We adopt two assumptions from Mori et al. (2018) for the $\delta^{18}\text{O}$ profile of KA01: 1) the meteoric water $\delta^{18}\text{O}$ is not related to the amount and seasonality of precipitation but changes with the seawater $\delta^{18}\text{O}$ and 2) the variability of the stalagmite $\delta^{18}\text{O}$ mainly depends on the temperature change. Assuming these, the temperature change can be reconstructed using stalagmite $\delta^{18}\text{O}$ values. First, the time series of the dripwater $\delta^{18}\text{O}$, $\delta^{18}\text{O}_w(t)$, is calculated with simple equations (2 and 3)

$$\delta^{18}\text{O}_w(t) = \delta^{18}\text{O}_w(0) + \delta^{18}\text{O}_{\text{SW}}(t) \quad (2)$$

$$\delta^{18}\text{O}_{\text{SW}}(t) = \Delta^{18}\text{O}_{\text{BF}}(t) / 1.77 \quad (3)$$

Here, $\delta^{18}\text{O}_w(0)$ represents the dripwater $\delta^{18}\text{O}$ at present, and we use the average value of -6.9‰ (VSMOW) for 2015 (Mori

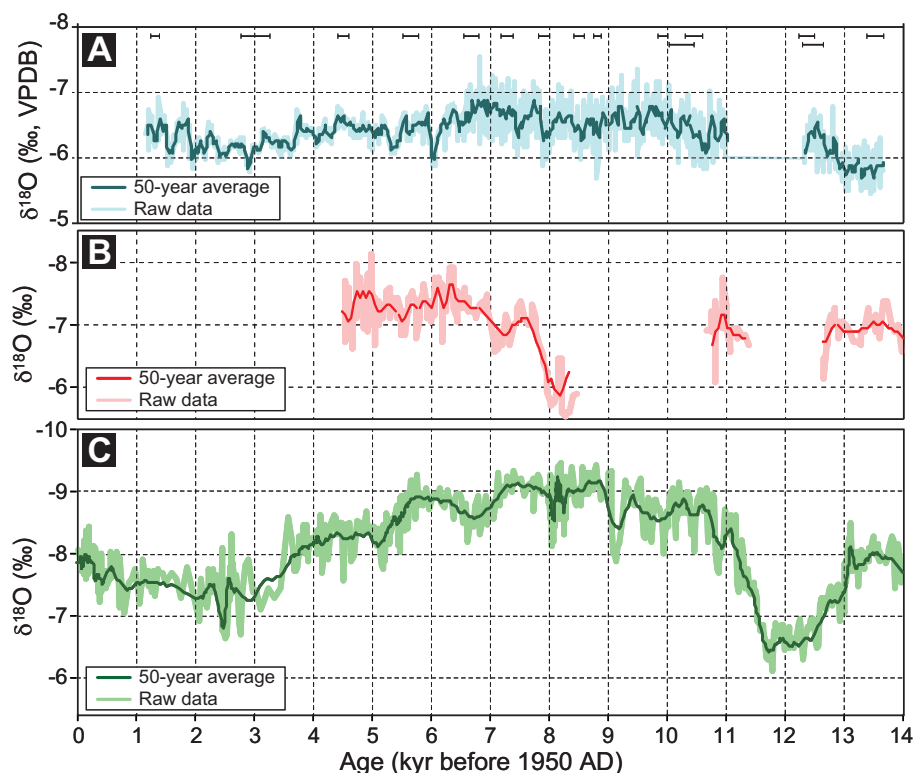


FIGURE 5 | Comparison of the stalagmite $\delta^{18}\text{O}$ profiles since 14 ka. Note that the vertical axis is reversed. (A) Kiriana Cave of this study. (B) Maboroshi Cave (locality is shown in Figure 1A) in Hiroshima Prefecture, Japan (Hori et al. 2013). (C) Dongge Cave in south China (Dykoski et al. 2005).

et al. 2018). $\delta^{18}\text{O}_{\text{SW}}(t)$ denotes the seawater $\delta^{18}\text{O}$ at a given time (t) quantified by the $\Delta^{18}\text{O}_{\text{BF}}(t)$, which is the difference between the present $\delta^{18}\text{O}$ value and the $\delta^{18}\text{O}$ value at the given time of deep Pacific benthic foraminifers. This difference decreases from the LGM to the present by 1.77‰ (Lisiecki and Stern 2016). $\delta^{18}\text{O}$ values of the foraminifers are primarily controlled by the variation of $\delta^{18}\text{O}_{\text{SW}}$ and secondarily by deep-water temperature. Considering that ^{18}O -enrichment in seawater during the LGM was around 1‰ (Schrage, Hampt, and Murray 1996; Schrage et al. 2002; Bintanja, and van de Wal, R.S.W. 2008; Shakun et al. 2015) and that the $\delta^{18}\text{O}_{\text{SW}}$ at present is 0‰, the $\Delta^{18}\text{O}_{\text{BF}}(t)$ divided by 1.77 is regarded as $\delta^{18}\text{O}_{\text{SW}}(t)$ (Equation 3).

Second, the time series of temperature in the cave is calculated from the $\delta^{18}\text{O}_{\text{W}}(t)$ and the measured stalagmite $\delta^{18}\text{O}(t)$ using the equation of Kim and O'Neil (1997):

$$1000 \ln \alpha = 18030 / T - 32.24 \quad (4)$$

where α is the fractionation factor between calcite and water, and T is the temperature in kelvins. The temperature (T) was reconstructed for $\delta^{18}\text{O}(t)$ with a 25-year time slice (dark green line of Figure 4A).

The calculated temperature ranges from 10.0°C to 15.0°C during Holocene (1.18–11.0 ka) and ranges from 11.5°C to 15.0°C during 12.4–13.7 ka (Figure 6A). The calculated temperature from the basal KA01 is around 12°C until 12.9 ka and then increases to ~15°C at 12.6 ka. From the maximum value, the temperature

decreases by 12.8°C at 12.4 ka. Across the 1.3-kyr-long hiatus, the temperature rapidly increased to 13.3°C until 10.9 ka. A high temperature of around 13°C sustains during an interval of 10.9–6.7 ka, although several changes with an amplitude of $\pm 1.0^\circ\text{C}$ are recorded in the temperature profile (Figure 6A). In this warm interval that may correspond to the Holocene Thermal Maximum (HTM; Kaufman et al. 2004), the stalagmite KA01 grew at a high rate (Figure 2B). A clear cooling started at 6.7 ka, and the temperature dropped to 10.5°C at 6.1 ka. Temperature remained in the range of 12°C–13°C from 6.0 ka to 3.8 ka and then decreased to 10.0°C at 2.9 ka, which is the lowest temperature in the Holocene period. The temperature gradually recovered to ~13°C to 1.2 ka when the stalagmite KA01 stopped its growth.

Figure 6B (in blue) also shows the temperatures estimated by the clumped isotopes (Δ_{47}), which include larger uncertainties and larger ranges (from 3.4°C to 16.2°C). Overall, the two temperature estimates (Δ_{47} and $\delta^{18}\text{O}$) share similar trends, with high temperatures in an interval of 7.8–6.5 ka and low temperatures in an interval of 4.5–2.0 ka. The Δ_{47} -temperatures are roughly consistent with the data reported from a stalagmite from Maboroshi Cave in Hiroshima Prefecture (Figure 1A) by Kato et al. (2021) (Figure 6B in orange), which also indicates a warm climate in the Middle Holocene (especially in an interval of 6.5–5.5 ka). These temperatures mainly range from 21°C to 15°C, clearly warmer than the present temperature (14.1°C, Kato et al. 2021) by 7°C–1°C (Figure 6B). It also shows a cool climate in the pre-Holocene section (14–12.5 ka; Figure 6B).

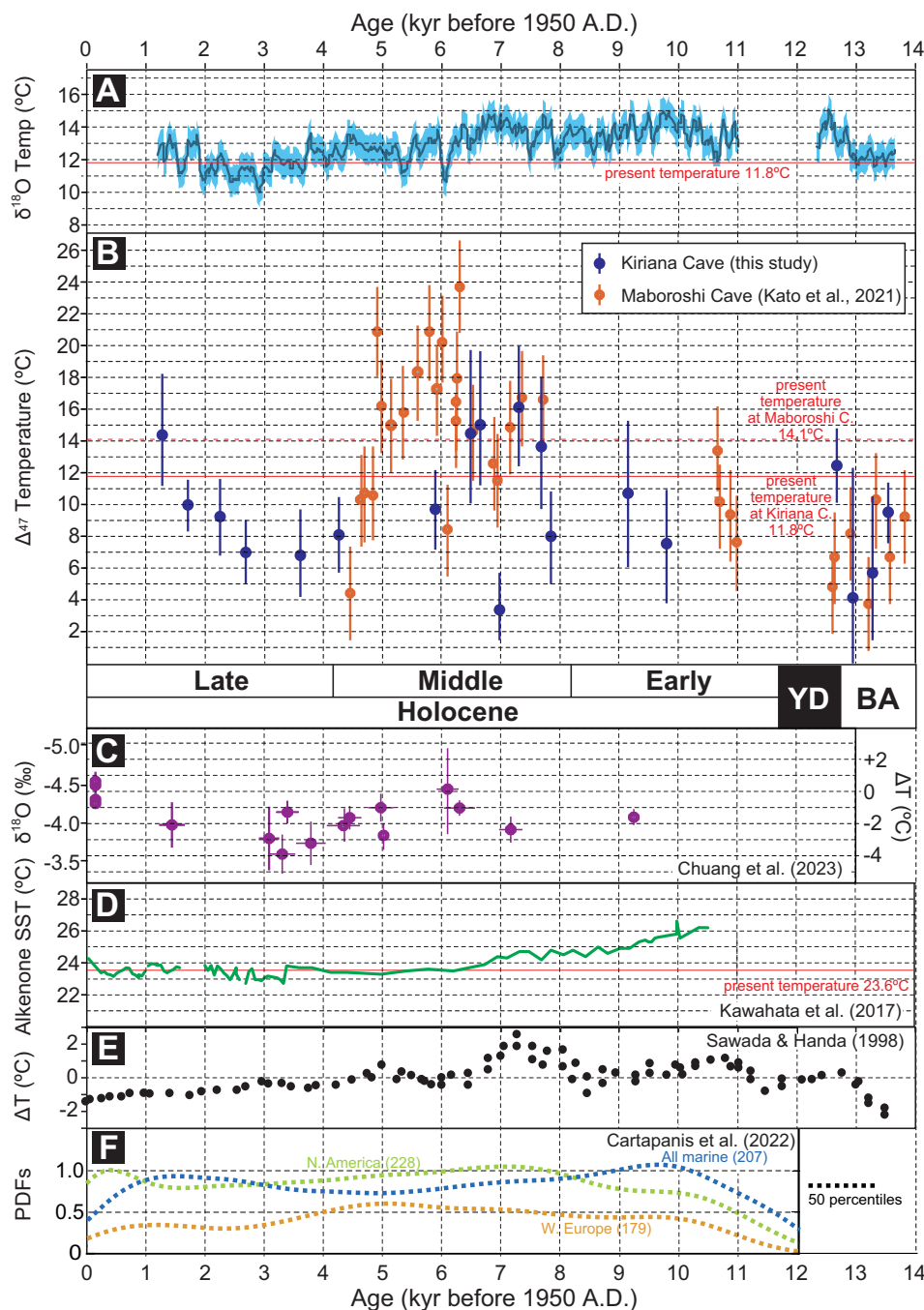
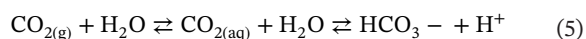


FIGURE 6 | Reconstructed temperature change since 14 ka from KA01 and other archives in Japan. (A) Temperature change reconstructed from $\delta^{18}\text{O}$ of KA01. (B) Δ_{47} temperatures of KA01 (this study) and a stalagmite collected from Maboroshi Cave in Hiroshima Prefecture (Kato et al. 2021). (C) $\delta^{18}\text{O}$ of reef corals from Kikai Island, Kagoshima Prefecture, and Okinawa Island, Okinawa Prefecture (compiled by Chuang et al. 2023). The temperature difference from the present was calculated by assuming the stable seawater $\delta^{18}\text{O}$. (D) C_{37} alkenone unsaturation-derived SST from sediment collected from Hiroshima Bay (Kawahata et al. 2017). (E) South–north latitudinal variations in temperature differences shown in Sawada and Handa (1998). These were calculated by subtracting C_{37} alkenone unsaturation-derived SSTs of sediment cores 31 $^{\circ}6' \text{N}$, 138 $^{\circ}40' \text{E}$ or 30 $^{\circ}23' \text{N}$, 138 $^{\circ}39' \text{E}$ from the corresponding values of another more northerly core (32 $^{\circ}40' \text{N}$, 138 $^{\circ}27' \text{E}$). (F) Probability density functions (PDFs) of Holocene Thermal Maximum (HTM) age calculated in Cartapanis et al. (2022). “Northern America” and “Western Europe” are continental data, and “All marine” is global data.

Although the two temperature estimates (Δ_{47} and $\delta^{18}\text{O}$) share similar features, a significant difference is observed in sections older than 9 ka, where the Δ_{47} temperature is much lower than the $\delta^{18}\text{O}$ -derived temperature. Because the pre-Holocene interval (13.7–12.3 ka) of KA01 corresponds to the Bølling–Allerød warm period and the first half of the Younger Dryas

cold period (e.g., Cheng et al. 2020), the temperature is expected to decrease to a level lower than the present temperature. To reconstruct lower $\delta^{18}\text{O}$ -derived temperatures, $\delta^{18}\text{O}_w(t)$ in Equation (2) for the pre-Holocene interval needs to be lower for some reasons. One possible reason is the lower $\delta^{18}\text{O}$ water vapor produced by lower sea surface temperatures (SSTs)

during the pre-Holocene period. It has been demonstrated that the warm Tsushima Current did not flow into the Japan Sea during 14–12.5 ka, resulting in further reduced SSTs (Domitsu and Oda 2006, 2008). Additionally, Nakagawa et al. (2021) suggested a southward shift of the westerly jet route during cold periods, including 14–12.5 ka, which increased the influx of air masses from the northwest and the Siberian High into the Japanese Islands. These air masses likely brought low $\delta^{18}\text{O}$ water vapor to Kiriana Cave due to the long trajectory from the vapor source to the cave. An increase in such air masses might have lowered $\delta^{18}\text{O}_{\text{w}}(t)$ in the pre-Holocene period around Kiriana Cave. Assuming that the meteoric water $\delta^{18}\text{O}$ was about 1‰ lower than $\delta^{18}\text{O}_{\text{w}}(t)$ in Equation (2), the calculated temperatures would have been about 4°C lower, consistent with the Δ_{47} temperatures. They are also different in the amplitude of the fluctuation, and the maximum difference of the Δ_{47} temperature change (12.8°C) is unrealistic for the Holocene section. This might be ascribed to the kinetic effect, as suggested by previous studies of carbonate clumped isotope thermometry (e.g., Guo and Zhou 2019; Dreybrodt 2019; Bajnai et al. 2020; Huntington and Petersen 2023). The kinetic effect on isotopic equilibrium also affects other isotopic compositions ($\delta^{18}\text{O}$ and $\delta^{13}\text{C}$) and mainly arises from the slow conversion rate between dissolved carbon dioxide ($\text{CO}_{2(\text{aq})}$) and bicarbonate (HCO_3^-) through hydration and hydroxylation reactions after CO_2 degassing (Guo and Zhou 2019)



The slow isotopic exchange between these carbonate species (Equation 5) does not achieve the equilibrium in a thin water film on a stalagmite and often lowers the Δ_{47} value in the case of stalagmites (Affek 2013; Affek et al. 2014). The degree of the isotopic disequilibrium is variable with various environmental parameters, including temperature, $p\text{CO}_2$, and dripwater supply (Affek and Zaarur 2014; Arienzo 2014; Arienzo et al. 2017; Bajnai et al. 2020; Hansen, Kluge, and Scholz 2022; Huntington and Petersen 2023). Potential indices available to estimate the kinetic effect are the growth rate and the Δ_{48} (abundance anomaly of mass 48 CO_2), shown in Table 2. Low Δ_{47} values (and high temperatures) are obtained from the samples of high growth rate and/or large Δ_{48} value, such as samples at 70- and 121-mm horizons (Table 2). However, the Δ_{47} values do not indicate a significant correlation with the high growth rate or the Δ_{48} value (Figure S2).

The lower Δ_{47} temperature trend persists throughout the stalagmite (Figure 6B), which might be attributable to the selection of the Δ_{47} -temperature equation. However, the Δ_{47} temperature becomes even lower by taking other equations, such as the tufa-based equation by Kato et al. (2019) and the travertine-based equation by Kele et al. (2015). Our data are not sufficient to estimate how the kinetic effect enlarges the variation of Δ_{47} temperature (Figure 6B), which is much larger than the variation of $\delta^{18}\text{O}$ temperature (Figure 6A). One possible explanation is that the Δ_{47} temperature suffers a larger kinetic effect (> 20°C, Affek et al. 2008, 2014) than the $\delta^{18}\text{O}$ temperature (~10°C, Tremaine, Froelich, and Wang 2011). In the case of applying the carbonate clumped isotopic thermometry to stalagmites, issues of a large kinetic effect need to be addressed (e.g., Affek et al. 2014). Considering a large variation and potential kinetic effect of the

Δ_{47} temperature, the $\delta^{18}\text{O}$ temperature indicates a more realistic trend than the Δ_{47} temperature. The Holocene trend of the $\delta^{18}\text{O}$ temperature shares several features with other temperature records in the Japanese Islands, as discussed in the next section (Figure 6).

4.3 | Temperature Change in Japanese Islands

Our temperature records from KA01 can be compared with previous studies that presented quantitative temperature reconstructions from well-dated geological materials. Kawahata et al. (2017) presented a high-resolution seawater temperature record from sediments in Hiroshima Bay, Hiroshima Prefecture (Figure 1A). The SSTs derived from C_{37} alkenone unsaturation indicate a gradual decrease from 26.5°C to 23.5°C during an interval of 10.5–6.2 ka. The SST stayed around 23.5°C for the next 3000 years, sharply decreased to 22.8°C at 3.3 ka, and then increased from 2.5 ka to 2.0 ka (Figure 6D). Oxygen isotope ratio profiles from reef corals from Kikai Island, Kagoshima Prefecture, and Okinawa Island, Okinawa Prefecture, over the past 9300-year show that SST increased by 2.5°C from 7.0 to 6.1 ka (Figure 6C, Chuang et al. 2023). The SST then declined slowly, reaching a cold event at 4–3 ka, taking a minimum of nearly 4°C below the present at 3.3 ka, and increasing toward the present. These SST profiles align well with the $\delta^{18}\text{O}$ -derived temperatures of Kiriana Cave, in terms of relatively warmer conditions in the early Holocene and the coolest conditions around 3 ka (Figure 6A). Climate change around 3 ka has also been reported from outside of Japan, such as from sediments of the Aegean Sea (Rohling et al. 2002) and the Greenland ice sheet (Mayewski et al. 1997; Meeker et al. 1997).

Based on the records of the stalagmite $\delta^{18}\text{O}$ of KA01, a relatively warm condition occurred around Kiriana Cave between 10.9 and 6.7 ka, reaching the highest temperature (15.0°C) around 7.0 ka, which is covered by the HTM. Compared with the global database of the HTM (Cartapanis et al. 2022; Kaufman and Broadman 2023), the timing found in KA01 aligns closely with seawater temperature records but is notably earlier than terrestrial records from North America and Western Europe, in which the HTM occurs around 7 ka and 5 ka, respectively (Figure 6F).

The earlier HTM observed at Kiriana Cave is likely due to its geographic proximity to the Pacific Ocean and the warm Kuroshio Current, combined with the absence of a large ice sheet. Sawada and Handa (1998), which reconstructed the historical flow path of the Kuroshio Current, suggested that the subtropical North Pacific circulation played a significant role in determining the velocity and degree of meandering of the Kuroshio Current. The strength of this circulation and the degree of meandering were estimated from SSTs reconstructed using sediment cores collected from three sites in the North Pacific off central Japan (Sawada and Handa 1998). Higher SSTs at the northern site, relative to the southern sites (indicated by a larger ΔT in Figure 6E), suggest reduced meandering of the Kuroshio Current, driven by an intensified subtropical North Pacific circulation. This oceanographic setting effectively transported heat and moisture from the tropics

to the mid-latitudes of the Pacific, which likely increased temperature and precipitation in the Kii Peninsula. According to Sawada and Handa (1998), the meandering of the Kuroshio Current was weak during 11–10 ka, so the Kii Peninsula was particularly affected by the Kuroshio Current, and the HTM began around 10 ka. Later, during 8–7 ka, the strength of the subtropical North Pacific circulation peaked (Figure 6E), resulting in the northward positioning and weakened meandering of the Kuroshio Current. During this period, EASM intensity reconstructed from Chinese stalagmite oxygen isotope ratios reached a maximum (Figure 5C), which was interpreted as the northward shift of the Intertropical Convergence Zone (Dykoski et al. 2005), and a warm and humid climate prevailed in East Asia. The temperature profile at Kiriana Cave around 6 ka shows a cold event (Figure 6A) when the Kuroshio meandering strengthened. After 5 ka, the meandering of the Kuroshio Current further strengthened (Figure 6E), and at the same time, the temperature at Kiriana Cave began to decrease. Around 3 ka, the Chinese stalagmite $\delta^{18}\text{O}$ reached a maximal value of about -7‰ , indicating that the EASM intensity weakened, and the period was dry (Figure 5C). Combined with the fact that Kiriana Cave has the lowest temperature, this cold and dry period may have contributed to the transition from the hunter-gatherer-oriented Jomon Period to the agriculture-oriented Yayoi Period. After 3 ka, the temperature began to increase, although the meandering of the Kuroshio Current slightly increased. This late Holocene temperature increase is also recorded in corals from Kikai Island (Figure 6C), alkenones from Hiroshima Bay (Figure 6D), and Chinese stalagmites, which suggest either a strengthening of the EASM or a northward shift of the ITCZ (Figure 5C). Thus, this warming trend appears to have been driven not by SSTs but rather by regional meteorological factors.

5 | Concluding Remarks

We reconstructed the temperature variability since 13.7 ka from the high-resolution $\delta^{18}\text{O}$ records of the well-dated stalagmite KA01 from Kiriana Cave in Mie Prefecture, Japan, under the assumption that the meteoric $\delta^{18}\text{O}$ is insensitive to the precipitation characteristics (the amount effect and the seasonality; Kano, Kato, and Murata 2023). KA01 provided high-resolution temperature records ranging from 10.0°C to 15.0°C , indicating warmer conditions in the early-middle Holocene during 10.9–6.7 ka and cooler conditions around 3 ka. These warm and cool intervals during the Holocene could be roughly supported by the temperature estimations from carbonate clumped isotopes (Δ_{47}) although the Δ_{47} temperature indicates a large amplitude of change. The temperature record based on $\delta^{18}\text{O}$ is also consistent with the other temperature records in Japan (e.g., Kato et al. 2021; Chuang et al. 2023; Kawahata et al. 2017) and the positioning of Kuroshio Current (Sawada and Handa 1998). We recognized that the HTM in Japan was earlier than those in Western Europe and North America. The amplitude of temperature variation estimated from $\delta^{18}\text{O}$ reaches $\sim 5^{\circ}\text{C}$, and it can be larger as estimated by the Δ_{47} data. Inconsistency is found in the $\delta^{18}\text{O}$ temperatures in the pre-Holocene section, which are much higher than the Δ_{47} temperature and previously reported paleotemperatures. This may indicate that our

assumption of the meteoric $\delta^{18}\text{O}$ cannot be applied to the pre-Holocene interval.

Because the meteoric $\delta^{18}\text{O}$ is insensitive to the precipitation characteristics in our study region, the stalagmite $\delta^{18}\text{O}$ signal of the Kiriana Cave possibly does not include information on precipitation. Reconstructing precipitation changes during the Holocene in response to temperature changes is an interesting topic in paleoclimatology. In particular, the reconstruction of precipitation phenomena during the early-middle Holocene, when it was warmer than now, will be useful for predicting natural disasters (e.g., floods and droughts) caused by global warming. Because the studied stalagmite, KA01, is a well-dated archive, further investigations of other proxies such as $\delta^{13}\text{C}$ and trace elements are needed to extract information on precipitation phenomena.

Acknowledgments

We would like to express our gratitude to Katsuji Yoshida for organizing the survey in Kiriana Cave. We also extend our thanks to Minoru Yoneda in Ohdai Town for collecting rainwater samples with great perseverance. Weather data were obtained from the website of the Japan Meteorological Agency (<http://www.jma.go.jp/>). This paper was improved by comments from the editor, Prof. Takashi Hasegawa, and two anonymous reviewers.

Conflicts of Interest

The authors declare no conflicts of interest.

Data Availability Statement

The data that supports the findings of this study are available in the [Supporting Information](#) of this article.

References

- Affek, H. P. 2013. "Clumped Isotopic Equilibrium and the Rate of Isotope Exchange Between CO_2 and Water." *American Journal of Science* 313, no. 4: 309–325.
- Affek, H. P., M. Bar-Matthews, A. Ayalon, A. Matthews, and J. M. Eiler. 2008. "Glacial/Interglacial Temperature Variations in Soreq Cave Speleothems as Recorded by 'Clumped Isotope' Thermometry." *Geochimica et Cosmochimica Acta* 72: 5351–5360.
- Affek, H. P., A. Matthews, A. Ayalon, et al. 2014. "Accounting for Kinetic Isotope Effects in Soreq Cave (Israel) Speleothems." *Geochimica et Cosmochimica Acta* 143: 303–318.
- Affek, H. P., and S. Zaarur. 2014. "Kinetic Isotope Effect in CO_2 Degassing: Insight from Clumped and Oxygen Isotopes in Laboratory Precipitation Experiments." *Geochimica et Cosmochimica Acta* 143: 319–330.
- Amekawa, S., K. Kashiwagi, M. Hori, et al. 2021. "Stalagmite Evidence for East Asian Winter Monsoon Variability and ^{18}O -Depleted Surface Water in the Japan Sea During the Last Glacial Period." *Progress in Earth and Planetary Science* 8: 1–15.
- Arienzo, M. 2014. "Subtropical Atlantic Climate Variability Record in Speleothems from the Bahamas." Ph.D. Dissertation. University of Miami. Florida.
- Arienzo, M. M., P. K. Swart, K. Broad, A. C. Clement, A. Pourmand, and B. Kakuk. 2017. "Multi-Proxy Evidence of Millennial Climate Variability From Multiple Bahamian Speleothems." *Quaternary Science Reviews* 161: 18–29.

- Bajnai, D., W. Guo, C. Spötl, et al. 2020. "Dual Clumped Isotope Thermometry Resolves Kinetic Biases in Carbonate Formation Temperatures." *Nature Communications* 11, no. 1: 4005.
- Baker, A., A. Hartmann, W. Duan, et al. 2019. "Global Analysis Reveals Climatic Controls on the Oxygen Isotope Composition of Cave Drip Water." *Nature Communications* 10, no. 1: 2984.
- Bar-Matthews, M., A. Ayalon, M. Gilmour, A. Matthews, and C. J. Hawkesworth. 2003. "Sea-Land Oxygen Isotopic Relationships From Planktonic Foraminifera and Speleothems in the Eastern Mediterranean Region and Their Implication for Paleorainfall During Interglacial Intervals." *Geochimica et Cosmochimica Acta* 67, no. 17: 3181–3199.
- Bintanja, R., and R. S. W. van de Wal. 2008. "North American Ice-Sheet Dynamics and the Onset of 100,000-Year Glacial Cycles." *Nature* 454: 869–872.
- Cartapanis, O., L. Jonkers, P. Moffa-Sanchez, S. L. Jaccard, and A. de Vernal. 2022. "Complex Spatio-Temporal Structure of the Holocene Thermal Maximum." *Nature Communications* 13, no. 1: 5662.
- Cheng, H., R. L. Edwards, A. Sinha, et al. 2016. "The Asian Monsoon Over the Past 640,000 Years and Ice Age Terminations." *Nature* 534, no. 7609: 640–646.
- Cheng, H., R. Lawrence Edwards, C. C. Shen, et al. 2013. "Improvements in ^{230}Th Dating, ^{230}Th and ^{234}U Half-Life Values, and U-Th Isotopic Measurements by Multi-Collector Inductively Coupled Plasma Mass Spectrometry." *Earth and Planetary Science Letters* 371–372: 82–91.
- Cheng, H., H. Zhang, C. Spo, et al. 2020. "Timing and Structure of the Younger Dryas Event and Its Underlying Climate Dynamics." *Proceedings of the National Academy of Sciences* 117, no. 38: 23408–23417.
- Chuang, K. Y., R. Asami, H. Takayanagi, et al. 2023. "Multidecadal-To-Interannual Modulations of Late Holocene Climate Variations Reconstructed From Oxygen Isotope Ratios of a 237-Year-Long Lived Fossil Coral in Kikai Island, Southwestern Japan." *Quaternary Science Reviews* 322: 108392.
- Dansgaard, W. 1964. "Stable Isotopes in Precipitation." *Tellus* 16: 438–468.
- Domitsu, H., and M. Oda. 2006. "Linkages Between Surface and Deep Circulations in the Southern Japan Sea During the Last 27,000 Years: Evidence From Planktic Foraminiferal Assemblages and Stable Isotope Records." *Marine Micropaleontology* 61, no. 4: 155–170.
- Domitsu, H., and M. Oda. 2008. "Holocene Influx of the Tsushima Current Into the Japan Sea Signalled by Spatial and Temporal Changes in *Neogloboquadrina incompta* Distribution." *Holocene* 18, no. 2: 345–352.
- Dreybrodt, W. 2019. "Implication to ^{13}C , ^{18}O , and Clumped $^{13}\text{C}^{18}\text{O}$ Isotope Composition in DIC and Calcite." *Acta Carsologica* 48, no. 1: 59–68.
- Dykoski, C. A., R. L. Edwards, H. Cheng, et al. 2005. "A High-Resolution, Absolute-Dated Holocene and Deglacial Asian Monsoon Record From Dongge Cave, China." *Earth and Planetary Science Letters* 233: 71–86.
- Fairchild, I. J., C. L. Smith, A. Baker, et al. 2006. "Modification and Preservation of Environmental Signals in Speleothems." *Earth-Science Reviews* 75: 105–153.
- Guo, W., and C. Zhou. 2019. "Patterns and Controls of Disequilibrium Isotope Effects in Speleothems: Insights From an Isotope-Enabled Diffusion-Reaction Model and Implications for Quantitative Thermometry." *Geochimica et Cosmochimica Acta* 267: 196–226.
- Hansen, M., T. Kluge, and D. Scholz. 2022. "Investigation of Disequilibrium Clumped Isotope Fractionation in (Speleothem) CaCO_3 With Cave Analogous Laboratory Experiments Using Thin Films of Flowing Solution." *Geochimica et Cosmochimica Acta* 321: 244–264.
- He, B., G. A. Olack, and A. S. Colman. 2012. "Pressure Baseline Correction and High-Precision CO_2 Clumped-Isotope (Δ_{47}) Measurements in Bellows and Micro-Volume Modes." *Rapid Communications in Mass Spectrometry* 26: 2837–2853.
- Hendy, C. H. 1971. "The Isotopic Geochemistry of Speleothems-I: The Calculations of the Effects of Different Modes of Formation on the Isotopic Composition of Speleothems and Their Applicability as Paleoclimate Indicators." *Geochimica et Cosmochimica Acta* 35: 801–824.
- Hiess, J., D. J. Condon, N. McLean, and S. R. Noble. 2012. " $^{238}\text{U}/^{235}\text{U}$ Systematics in Terrestrial Uranium-Bearing Minerals." *Science* 335: 1610–1614.
- Hori, M., T. Ishikawa, K. Nagaishi, et al. 2013. "Prior Calcite Precipitation and Source Mixing Process Influenced Sr/Ca, Ba/Ca and $^{87}\text{Sr}/^{86}\text{Sr}$ of a Stalagmite Developed in Southwestern Japan During 18.0–4.5 ka." *Chemical Geology* 347: 190–198.
- Hori, M., T. Kawai, J. Matsuoka, and A. Kano. 2009. "Intra-Annual Perturbations of Stable Isotopes in Tufas: Effects of Hydrological Processes." *Geochimica et Cosmochimica Acta* 73, no. 6: 1684–1695.
- Huntington, K. W., and S. V. Petersen. 2023. "Frontiers of Carbonate Clumped Isotope Thermometry." *Annual Review of Earth and Planetary Sciences* 51, no. 1: 611–641.
- Ishizuka, M., Y. Sone, H. Ii, and T. Hirata. 2004. "Rainfall-Topography Effect on Spatial Distribution of Stable Isotope Ratios of Surface Water in Kii Peninsula." *Proceedings of Hydraulic Engineering* 48: 235–240.
- Jaffey, A. H., K. F. Flynn, L. E. Glendenin, W. C. Bentley, and A. M. Essling. 1971. "Precision Measurement of Half-Lives and Specific Activities of ^{235}U and ^{238}U ." *Physical Review Section C4*: 1889–1906.
- Kano, A., H. Kato, and A. Murata. 2023. "Oxygen Isotopes of the Japanese Stalagmites as Global and Local Paleoclimate Proxies." *Island Arc* 32, no. 1: e12491.
- Kano, A., T. Okumura, C. Takashima, and F. Shiraishi. 2019. "Travertines in Japan." In *Geomicrobiological Properties and Processes of Travertine: With a Focus on Japanese Sites*. Singapore: Springer Nature.
- Kashiwagi, K., K. Yoshida, and Y. Inagaki. 2007. "Subsurface Geology of Kiri-Ana Cave (Limestone Cave) and Geological Structure of the Aso Karst in the Eastern Kii Peninsula, Southwest Japan (Preliminary report)." *Memoir of the Fukui Prefectural Dinosaur Museum* 6: 35–44. (In Japanese with English abstract).
- Kato, H., S. Amekawa, A. Kano, T. Mori, Y. Kuwahara, and J. Quade. 2019. "Seasonal Temperature Changes Obtained From Carbonate Clumped Isotopes of Annually Laminated Tufas From Japan: Discrepancy Between Natural and Synthetic Calcites." *Geochimica et Cosmochimica Acta* 244: 548–564.
- Kato, H., T. Mori, S. Amekawa, et al. 2021. "Influences of Temperature and the Meteoric Water $\delta^{18}\text{O}$ Value on a Stalagmite Record in the Last Deglacial to Middle Holocene Period From Southwestern Japan." *Quaternary Science Reviews* 253: 106746.
- Kato, H., T. Mori, S. Amekawa, C.-C. Wu, C.-C. Shen, and A. Kano. 2023. "Coevolutions of Terrestrial Temperature and Monsoonal Precipitation Amounts From the Latest Pleistocene to the Mid-Holocene in Japan: Carbonate Clumped Isotope Record of a Stalagmite." *Chemical Geology* 622: 121390.
- Kaufman, D. S., T. A. Ager, N. J. Anderson, et al. 2004. "Holocene Thermal Maximum in the Western Arctic (0–180°W)." *Quaternary Science Reviews* 23, no. 5–6: 529–560.
- Kaufman, D. S., and E. Broadman. 2023. "Revisiting the Holocene Global Temperature Conundrum." *Nature* 614, no. 7948: 425–435.
- Kawahata, H., M. Matsuoka, A. Togami, et al. 2017. "Climatic Change and Its Influence on Human Society in Western Japan During the Holocene." *Quaternary International* 440: 102–117.
- Kawahata, H., H. Ohshima, and A. Kuroyanagi. 2011. "Terrestrial—Ocean Environmental Change in the Northwestern Pacific From

- the Glacial Times to Holocene." *Journal of Asian Earth Sciences* 40: 1189–1202.
- Kele, S., S. F. Breitenbach, E. Capezzuoli, et al. 2015. "Temperature Dependence of Oxygen and Clumped Isotope Fractionation in Carbonates: A Study of Travertines and Tufas in the 6–95°C Temperature Range." *Geochimica et Cosmochimica Acta* 168: 172–192.
- Kigoshi, T., F. Kumon, R. Hayashi, M. Kuriyama, K. Yamada, and K. Takemura. 2014. "Climate Changes for the Past 52 ka Clarified by Total Organic Carbon Concentrations and Pollen Composition in Lake Biwa, Japan." *Quaternary International* 333: 2–12.
- Kim, S. T., and J. R. O'Neil. 1997. "Equilibrium and Nonequilibrium Oxygen Isotope Effects in Synthetic Carbonates." *Geochimica et Cosmochimica Acta* 61: 3461–3475.
- Lisiecki, L. E., and J. V. Stern. 2016. "Regional and Global Benthic $\delta^{18}\text{O}$ Stacks for the Last Glacial Cycle." *Paleoceanography* 31: 1368–1394.
- Liu, Z. Y., X. Y. Wen, E. C. Brady, et al. 2014. "Chinese Cave Records and the East Asia Summer Monsoon." *Quaternary Science Reviews* 83: 115–128.
- Mayewski, P. A., L. D. Meeker, M. S. Twickler, et al. 1997. "Major Features and Forcing of high-latitude Northern Hemisphere Atmospheric Circulation Using a 110,000-Year Long Glaciochemical Series." *Journal of Geophysical Research* 102: 26345–26366.
- McDermott, F. 2004. "Palaeo-Climate Reconstruction From Stable Isotope Variations in Speleothems: A Review." *Quaternary Science Reviews* 23: 901–918.
- Meeker, L. D., P. A. Mayewski, M. S. Twickler, S. I. Whitlow, and D. Meese. 1997. "A 110,000-Year History of Change in Continental Biogenic Emissions and Related Atmospheric Circulation Inferred From the Greenland Ice Sheet Project Ice Core." *Journal of Geophysical Research* 102: 26489–26504.
- Mori, T., K. Kashiwagi, S. Amekawa, et al. 2018. "Temperature And Seawater Isotopic Controls on Two Stalagmite Records Since 83 ka From Maritime Japan." *Quaternary Science Reviews* 192: 47–58.
- Nakagawa, T., P. Tarasov, Staff, R., et al. 2021. "The Spatio-Temporal Structure of the Lateglacial to Early Holocene Transition Reconstructed From the Pollen Record of Lake Suigetsu and Its Precise Correlation With Other Key Global Archives: Implications for Palaeoclimatology and Archaeology." *Global and Planetary Change* 202: 103493.
- Nakagawa, T., P. E. Tarasov, K. Nishida, K. Gotanda, and Y. Yasuda. 2002. "Quantitative Pollen-Based Climate Reconstruction in Central Japan: Application to Surface and Late Quaternary Spectra." *Quaternary Science Reviews* 21: 2099–2113.
- Pausata, F. S. R., D. S. Battisti, K. H. Nisancioglu, and C. M. Bitz. 2011. "Chinese Stalagmite $\delta^{18}\text{O}$ Controlled by Changes in the Indian Monsoon During a Simulated Heinrich Event." *Nature Geoscience* 4, no. 7: 474–480.
- Rohling, E. J., P. A. Mayewski, A. Hayes, R. H. Abu-Zied, and J. S. L. Casford. 2002. "Holocene Atmosphere–Ocean Interactions: Records From Greenland and the Aegean Sea." *Climate Dynamics* 18: 573–592.
- Rozanski, K., L. Araguás-Araguás, and R. Gonfiantini. 1993. "Isotopic Patterns in Modern Global Precipitation." In *Climate Change in Continental Isotopic Records*, edited by P. K. Swart, K. L. Lohmann, J. McKenzie, and S. Savin, 1–37. Washington: American Geophysical Union. Geophysical Monograph, 78.
- Sawada, K., and N. Handa. 1998. "Variability of the Path of the Kuroshio Ocean Current Over the Past 25,000 Years." *Nature* 392: 592–595. <https://doi.org/10.1038/33391>.
- Scholz, D., and D. L. Hoffmann. 2011. "StalAge—An Algorithm Designed for Construction of Speleothem Age Models." *Quaternary Geochronology* 6: 369–382.
- Schrag, D. P., J. F. Adkins, K. McIntyre, et al. 2002. "The Oxygen Isotopic Composition of Seawater During the Last Glacial Maximum." *Quaternary Science Reviews* 21: 331–342.
- Schrag, D. P., G. Hampt, and D. W. Murray. 1996. "The Temperature and Oxygen Isotopic Composition of the Glacial Ocean." *Science* 272: 1930–1932.
- Shakun, J. D., D. W. Lea, L. E. Lisiecki, and M. E. Raymo. 2015. "An 800-kyr Record of Global Surface Ocean $\delta^{18}\text{O}$ and Implications for Ice Volume-Temperature Coupling." *Earth and Planetary Science Letters* 426: 58–68.
- Shen, C.-C., A. Kano, M. Hori, K. Lin, T.-C. Chiu, and G. B. Burr. 2010. "East Asian Monsoon Evolution and Reconciliation of Climate Records From Japan and Greenland During the Last Deglaciation." *Quaternary Science Reviews* 29: 3327–3335.
- Shen, C.-C., R. Lawrence Edwards, H. Cheng, et al. 2002. "Uranium and Thorium Isotopic and Concentration Measurements by Magnetic Sector Inductively Coupled Plasma Mass Spectrometry." *Chemical Geology* 185: 165–178.
- Shen, C. C., K. S. Li, K. Sieh, et al. 2008. "Variation of Initial $^{230}\text{Th}/^{232}\text{Th}$ and Limits of High Precision U-Th Dating of Shallow-Water Corals." *Geochimica et Cosmochimica Acta* 72, no. 17: 4201–4223.
- Shen, C. C., C. C. Wu, H. Cheng, et al. 2012. "High-Precision and High-Resolution Carbonate ^{230}Th Dating by MC-ICP-MS With SEM Protocols." *Geochimica et Cosmochimica Acta* 99: 71–86.
- Suzuki, K., K. Mimura, S. Inagaki, and M. Takeuchi. 2015. "Coniform Conodonts Collected From the Aso Limestone Body in the Chichibu Belt, Mie Prefecture." *Journal of the Geological Society of Japan* 121: 179–183. (In Japanese With English Abstract).
- Tremaine, D. M., P. N. Froelich, and Y. Wang. 2011. "Speleothem Calcite Farmed In Situ: Modern Calibration of $\delta^{18}\text{O}$ and $\delta^{13}\text{C}$ Paleoclimate Proxies in a Continuously-Monitored Natural Cave System." *Geochimica et Cosmochimica Acta* 75, no. 17: 4929–4950.
- Uemura, R., M. Nakamoto, R. Asami, et al. 2016. "Precise Oxygen and Hydrogen Isotope Determination in Nanoliter Quantities of Speleothem Inclusion Water by Cavity Ring-Down Spectroscopic Techniques." *Geochimica et Cosmochimica Acta* 172: 159–176.
- Walker, M., M. J. Head, M. Berkelhammer, et al. 2018. "Formal Ratification of the Subdivision of the Holocene Series/Epoch (Quaternary System/Period): Two New Global Boundary Stratotype Sections and Points (GSSPs) and Three New Stages/Subseries." *Episodes Journal of International Geoscience* 41, no. 4: 213–223.
- Wang, H., J. Chen, X. Zhang, and F. Chen. 2014. "Palaeosol Development in the Chinese Loess Plateau as an Indicator of the Strength of the East Asian Summer Monsoon: Evidence for a Mid-Holocene Maximum." *Quaternary International* 334–335: 155–164.
- Wang, Y., H. Cheng, R. L. Edwards, et al. 2001. "A High-Resolution Absolute-Date Late Pleistocene Monsoon Record From Hulu Cave, China." *Science* 294: 2345–2348.
- Wang, Y., H. Cheng, R. L. Edwards, et al. 2008. "Millennial- and Orbital-Scale Changes in the East Asian Monsoon Over the Past 224,000 Years." *Nature* 451: 1090–1093.
- Yang, X. L., J. B. Liu, F. Y. Liang, D. X. Yuan, Y. Yang, and F. H. Chen. 2014. "Holocene Stalagmite $\delta^{18}\text{O}$ Records in the East Asian Monsoon Region and Their Correlation With Those in the Indian Monsoon Region." *Holocene* 24: 1657–1664.

Supporting Information

Additional supporting information can be found online in the Supporting Information section.